Journal of Biomedical Optics

BiomedicalOptics.SPIEDigitalLibrary.org

Sensorless adaptive optics implementation in widefield optical sectioning microscopy inside *in vivo Drosophila* brain

Mélanie Pedrazzani
Vincent Loriette
Paul Tchenio
Sakina Benrezzak
Daniele Nutarelli
Alexandra Fragola

SPIE.

Mélanie Pedrazzani, Vincent Loriette, Paul Tchenio, Sakina Benrezzak, Daniele Nutarelli, Alexandra Fragola, "Sensorless adaptive optics implementation in widefield optical sectioning microscopy inside *in vivo Drosophila* brain," *J. Biomed. Opt.* **21**(3), 036006 (2016), doi: 10.1117/1.JBO.21.3.036006.

Sensorless adaptive optics implementation in widefield optical sectioning microscopy inside *in vivo Drosophila* brain

Mélanie Pedrazzani,[a] Vincent Loriette,[b,*] Paul Tchenio,[a,c] Sakina Benrezzak,[a] Daniele Nutarelli,[a] and Alexandra Fragola[b]
[a]Université Paris-Saclay, Laboratoire Aimé Cotton, CNRS, Université Paris-Sud, ENS Cachan, Orsay Cedex 91405, France
[b]CNRS, Laboratoire de Physique et d'Étude des Matériaux, ESPCI, 10 Rue Vauquelin, Paris 75005, France
[c]CNRS, Gènes et Dynamiques des Systèmes de Mémoire, Unité de Neurobiologie, ESPCI, 10 Rue Vauquelin, Paris 75005, France

Abstract. We present an implementation of a sensorless adaptive optics loop in a widefield fluorescence microscope. This setup is designed to compensate for aberrations induced by the sample on both excitation and emission pathways. It allows fast optical sectioning inside a living *Drosophila* brain. We present a detailed characterization of the system performances. We prove that the gain brought to optical sectioning by realizing structured illumination microscopy with adaptive optics down to 50 μm deep inside living *Drosophila* brain. [DOI: 10.1117/1.JBO.21.3.036006]

Keywords: adaptive optics; structured illumination microscopy; biological imaging.

Paper 150748RR received Nov. 7, 2015; accepted for publication Feb. 11, 2016; published online Mar. 11, 2016.

1 Introduction

Fluorescence microscopy is the technique of choice for *in vivo* functional imaging when micrometric spatial resolution and high sensitivity are required. Among different imaging techniques that can be used for fast *in vivo* dynamic studies,[1,2] we have chosen a widefield approach, as it requires low excitation power density and provides efficient use of the excitation photons. However, when imaging deep inside biological tissues, its performances are strongly limited by out-of-focus fluorescence emission. Optical sectioning using structured illumination, such as HiLo microscopy (for high and low spatial frequencies), efficiently overcomes this limitation while preserving high frame rate as it only requires two images to be acquired.[2] A uniform illumination image provides the high-frequency content of the optical section. The in-focus low-frequency content is extracted from a processed image acquired with a structured illumination.[3] HiLo microscopy capability to provide high-resolution images *in vivo* into the *Drosophila* brain has already been demonstrated[4] but was limited to near-surface imaging due to the decrease of the contrast of the illumination pattern deep inside the brain. This contrast degradation is due to light scattering, which induces a high background and to wavefront distortion by the aberrant nature of the tissue structures. In order to build optical sections, it is mandatory to have a high contrast of the illumination pattern in the microscope object plane, so it is essential to preserve it when imaging deeper than 20 μm. We chose to correct the sample-induced aberrations by shaping the wavefront with a deformable mirror (DM).[5–7] Two main strategies have been recently developed for adaptive optics implementation on widefield fluorescent microscopes: correction either using a measured wavefront coming from a "star" inside the sample[8–10] or by estimating a merit factor in the acquired image.[11] As in our case, it was not possible to insert fluorescent beacons within the living *Drosophila* brain, so we implemented a sensorless approach with an image-based optimization method. This approach is certainly slower than guide star-based wavefront correction optimization, but it does not add constraints to the sample preparation and turns to be more versatile as it does not rely on the position of a given beacon and can be easily targeted on a region of interest in the sample.

In this article, we will show that it is not possible to use patterned illumination methods deeper than 20 μm inside the *Drosophila* brain without correcting the aberrations induced by the sample. We will then prove that by implementing an adaptive optics loop with its wavefront shaping element placed in a location common to the excitation and emission paths, we are able to preserve the contrast of the illumination pattern and provide aberration-corrected fluorescence images at depths down to 50 μm. We will discuss the choice of the optimization criterion to optimize the excitation and emission optical pathways. The characterization of our setup will give us estimates of the largest area that may be corrected of its aberrations, the thickness and the duration over which a given wavefront aberration can be maintained to recover good quality fluorescence images. We will then compare optical sections obtained using the HiLo technique for different levels of correction. We will end by discussing some strategies that could be implemented for high-speed three-dimensional (3-D) imaging into living brain.

2 Material and Methods

2.1 *Biological Sample Preparation*

Flies carrying the genetically encoded fluorescent probes UAS-CD8-GFP were crossed with 238Y-Gal4 flies to drive green fluorescent protein expression (GFP; emission peak at

*Address all correspondence to: Vincent Loriette, E-mail: vincent.loriette@espci.fr

1083-3668/2016/$25.00 © 2016 SPIE

510 nm) in all mushroom bodies intrinsic neurons, so-called Kenyon cells, due to the UAS-Gal4 system.[12] The flies were reared at a controlled temperature of 25°C. For *in vivo* imaging, 3- to 5-day-old fly was glued by the dorsal part of its head and thorax on a plastic film. A small aperture was made in the plastic film at the level of the head to remove the underlying cuticle and trachea according to standard procedure.[13] The brain was bathed during all the experiments with physiological Ringer's solution containing (in mM) 130 NaCl, 5 KCl, 36 $C_{12}H_{22}O_{11}$ sucrose, 2 $MgCl_2$, 2 $CaCl_2$, and 5 HEPES NaOH (pH = 7.3). In order to prevent most movements of the brain, we put in place an agarose gel (A9414, Sigma Aldrich, 2% massic concentration) above the brain. A rough estimate of the residual movements was a few micrometers with a typical frequency of 1 Hz. After the experiment, we checked that the fly was still alive by looking its response to mechanical stimulation (like movement of legs in response to air flow).

2.2 *Optical Device*

We chose to build our microscope starting from a commercial microscope stage, as it provides excellent mechanical stability, numerous readily available optical ports, and an optimized optical design. As our goal was to simultaneously correct the aberrations induced by the sample and the aberrations present in the illumination path, we inserted a DM at a location common to excitation and emission.

Our microscope design is shown in Fig. 1. The setup is based on a commercial inverted fluorescence microscope (Olympus IX 71). The 15-mm-diameter DM (Imagine Optic, Mirao e52) was placed in a plane conjugate of the microscope objective exit pupil (Leica, Fluotar 25×, 0.95 W). As can be seen in Fig. 1, the DM lied at a location common to excitation and emission pathways, in order to correct the aberrations present in the imaging path, as well as aberrations present between the patterning element and the sample. Design constraints led to place the DM slightly tilted with respect to the optical axis. We did not find experimental evidence that this tilt has any effect on the efficiency of the wavefront correction. The first afocal arrangement allowed the DM to be placed outside of the microscope body, and the second afocal was used to match 87% of the size of the DM to the size of the objective pupil. We built the two telescopes using commercially available 1-in. diameter achromatic doublets. A digital micromirror device (DMD, Texas Instruments Discovery 4100 0.7 XGA) conjugate of the objective front focal plane of the microscope objective was used to pattern the excitation light (cube laser 488 nm 50 mW, coherent). A diffuser was used to reduce the spatial coherence of the laser source in order to provide speckle-free illumination. The axial position of the image of the DMD projected in the sample was set by adjusting the length and position of the telescope, which conjugates the DMD to the microscope field diaphragm. Laser excitation and fluorescence emission were split by a dichroic filter (DF) and a high-pass filter (Z488RDC and 500LP from Chroma Technology) within the microscope stage. Fluorescence images were recorded on a complementary metal-oxide semiconductor camera (Hammamatsu, Orca-Flash 4.0) plugged on the triocular microscope head. The emission light could be directed on a Shack–Hartmann wavefront sensor (WS, Imagine Optic, Haso3 first), conjugate of the DM, due to a flipping mirror. The lens placed in front of the WS, used

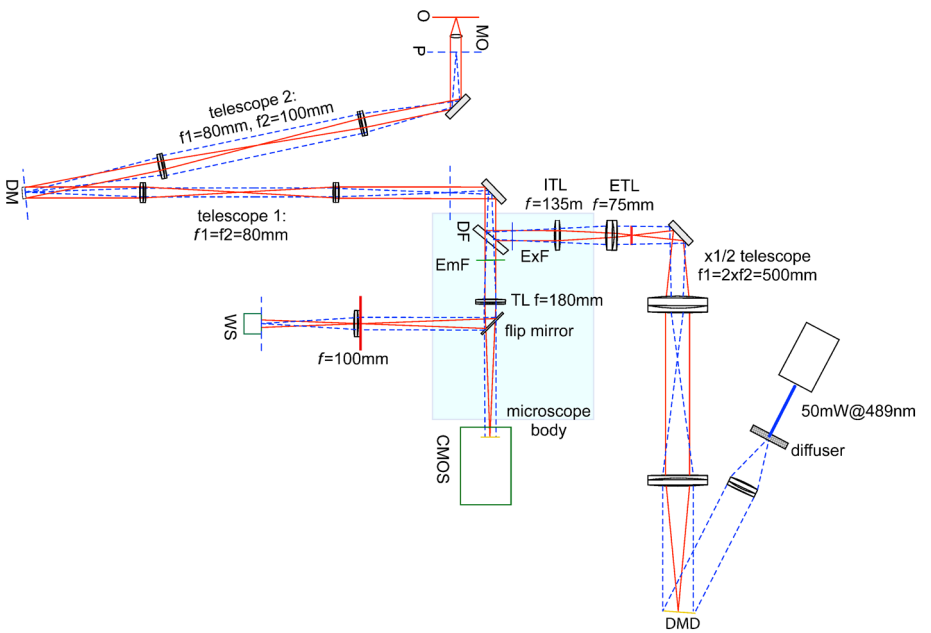

Fig. 1 Microscope setup. The setup can be decomposed in different parts. The excitation part is composed of the diode laser and the digital micromirror device (DMD) to create a structured illumination. The aberration correction part includes the DM in a plane conjugated to the pupil of the objective in a place common to excitation and detection. A complementary metal-oxide semiconductor (CMOS) camera is used to image fluorescence signals. The Shack–Hartmann WS is only used to correct static aberrations of the setup prior to imaging and create required matrix command to run the optimization algorithm. The blue and red lines correspond to planes conjugate of the DM and to the object plane, respectively. The notations MO, TL, DF, P, O, ETL, ITL, ExF, and EmF are used for microscope objective, tube lens, dichroic filter, pupil plane, object plane, external tube lens, illumination tube lens, excitation filter, and emission filter, respectively.

to conjugate the WS to the DM, was not part of the excitation or emission path. It was placed in a plane conjugate of the sample. Therefore, this field lens affected the wavefront only to a low extent. The WS was employed only during the initial setup phase but it was not used during the optimization process.

2.3 *Optimization Algorithm*

We used the optimization algorithm software MicAO provided by Imagine Optic company and developed a merit factor adapted to structured illumination microscopy. The optimization process aims at minimizing a merit factor computed from the acquired images, by sequentially compensating the wavefront aberrations, these aberrations being decomposed on the classical Zernike basis. Starting from an initial mirror shape, a fixed amount of a single aberration was added and then subtracted. We thus measured three values of the merit factor for each aberration. A parabolic fit allowed one to find the best mirror shape to compensate this particular aberration. The next aberration was compensated the same way, this time starting with the mirror shape obtained previously. We compensated all the third-order aberrations except defocus, tip and tilt. Only the fifth-order spherical aberration was corrected because we observed that compensating the other fifth-order aberrations did not improve the quality of the images. We recorded the DM shape when correcting all third- and fifth-order aberrations and compared it with the shape obtained when correcting all third-order aberrations and only fifth-order spherical aberration. The difference between the two corresponding wavefronts was lower than 10-nm RMS. We did not use a basis specifically designed for a particular merit function, so it was not guaranteed that at the end of the optimization step, the best mirror shape is obtained. However, we verified that the final value of the merit factor did not depend on the number of optimization runs we performed. So, even if our aberration basis is not orthogonal for a given merit factor, it was suitable enough to lead to improvements throughout the optimization process. The improvement of the wavefront quality obtained using this basis was sufficient for our application, but we cannot guarantee that we were able to obtain the best wavefront improvement. The choice of the merit function strongly depends on the sample characteristics and the illumination technique.[14] When testing our setup with fluorescent beads, we could use standard merit factors like Sobel or Laplace, which are sensitive to local gradients and edges.[15] In the case of *in vivo* imaging of *Drosophila* brains, we recorded very noisy images with weak contrasts and no sharp discontinuities because of high out-of-focus fluorescence background, so Sobel- or Laplace-based optimizations usually failed. As we did not use isolated guide stars and wished to perform wide-field optimization, we had to generate some measurable information in the sample in order to feed the merit factor. The patterned illumination by a grid is well adapted as we know what should be its image in absence of aberration. The illumination-based merit factor is defined as the integral of the power spectral density of each image in Gaussian windows centered on the peaks of Fourier spectrum of the illumination pattern. The merit factor M is computed by

$$M = \left(\iint |G(f_x, f_y)\mathcal{F}(I)|^2 \mathrm{d}f_x \mathrm{d}f_y \right)^{-1}, \quad (1)$$

where $\mathcal{F}(I)$ is the Fourier transform of the image I, G is a Gaussian filter of width w centered on the spatial frequency $(f_{x,\mathrm{mod}}, f_{y,\mathrm{mod}})$ of the pattern, i.e.,

$$G(f_x, f_y) = \exp\left[-\frac{(f_x - f_{x,\mathrm{mod}})^2 + (f_y - f_{y,\mathrm{mod}})^2}{w^2} \right]. \quad (2)$$

Optimizing this merit factor M is equivalent to maximizing the contrast of the pattern imaged on the camera. The choice of the spatial frequency of the illumination pattern is dictated by two opposite constraints: if the frequency is high, close to the microscope cutoff frequency, the contrast of the pattern is low, the merit function gets very noisy, and it becomes difficult for the optimization algorithm to converge. On the other hand, if the frequency of the pattern is low, then the bandwidth of the in-focus low-frequency content recovered by the HiLo algorithm becomes very limited and very little low-frequency information is present in the optical section. Moreover, the period of the pattern has to be chosen much smaller than the size of the region of interest in the images. In practice, we worked with pattern periods ranging between 1 and 4 μm. These values correspond to spatial frequencies ranging between 7% and 29% of the microscope cutoff frequency. Ideally, we should have chosen to work at half the cutoff frequency, where the optical sectioning has the lowest depth of focus,[16] but we did not succeed to obtain a sufficiently high contrast in this configuration when imaging deeper than 20 μm inside the *Drosophila* brain. The efficiency of the optimization algorithm depends on the Gaussian filter width w. This width was chosen empirically, its value was close to 2% of the microscope cutoff frequency.

The optimization method is useful for correcting the unpredictable aberrations induced by the sample. Aberrations induced by the setup in the path common to the emission and the excitation, between the microscope objective and the dichroic mirror, were estimated and corrected using DM and WS in a closed-loop configuration and calibrated fluorescent beads as guide stars. The mirror shape obtained at this stage was then used as the starting shape for the optimization processes. Decoupling the compensation of the aberrations present in the optical system from the aberrations induced by the sample greatly facilitates the efficiency of the image-based optimization algorithm by providing an initial guess. We call this initial DM shape the "best flat mirror." This shape required only typically 10% of the dynamic range of the DM. It must be noted, however, that the recording of this mirror map was not mandatory to perform the sensorless optimization. Its use allowed us to start the optimization by having already corrected the setup induced aberrations. We need to record a command matrix to drive the DM. Indeed, the sensorless algorithm uses mirror deformations that match the Zernike aberrations, so it has to know how the commands sent to the DM translate to its final shape. We chose to use a WS to calculate the DM control matrix,[17] although this step could be done without this element.[18] During the course of the sensorless optimization, the WS was not used. In practice, the command matrix is computed daily in order to compensate any mechanical drift of the microscope.

3 Characterization and Performances of the Setup

3.1 *Evaluation of the Differential Aberration in the Excitation and Emission Paths*

As we use patterned excitation in order to build optical sections, the DM mirror has to compensate simultaneously the aberrations present in the excitation path, in order to provide a

good pattern contrast in the sample and in the emission path in order to recover aberration-free images. However, these paths are only common between the dichroic mirror and the sample. It is relevant to ensure that no differential aberration between the emission and excitation is present. The presence of differential aberrations along the two paths would limit the dynamics of the optimization. In order to evaluate the differential aberrations between the excitation and emission paths, we imaged a dense stripe of 1-μm-diameter green fluorescent beads deposited on a coverslip and performed two different optimization steps, one using a merit function based on the Fourier factor of merit and the second based on the Sobel factor of merit. The Fourier merit factor is mostly sensitive to aberrations present between the DMD and the camera. Optimization using this merit factor corrects full path composed of the excitation and emission paths. The Sobel merit factor is sensitive to sharp discontinuities in the image, like the edges of the bead images. Optimization based on the Sobel factor thus corrects only the emission path. If no differential aberration is present, the two optimizations should lead to the same DM shape. In Fig. 2, we show the images obtained after optimization either with Sobel merit factor [Fig. 2(a)] or with Fourier merit factor [Fig. 2(b)]. By comparing the DM shapes for the two optimizations, we measured a 20-nm RMS differential aberration between excitation and emission paths [Figs. 2(c) and 2(d)]. This value is not significant as it corresponds to the fluctuations of the merit factor. This result proves that differential aberrations do not play a significant role in the efficiency of the aberration reduction.

3.2 *Evaluation of Spatial Lateral Extent of Correction*

Some authors[19] have proved that placing the DM at other locations than conjugate to the exit pupil of the objective would lead to a more efficient compensation of the aberrations induced by the samples. However, this is true if the axial positions of the aberrant regions are known. We did not have this *a priori* knowledge, so we decided to work in the most common configuration. This means that the wavefront we wish to correct is the average of all the wavefronts coming by all the emitting regions in the field of view. If the sample is inhomogeneous, as it is the case with *Drosophila* brain, then the optimization loop, acting on a single DM, will not be able to compensate all the wavefront distortions throughout the whole sample. It thus may not be a clever choice to build our merit factor from the whole image, but rather use a smaller area inside of which we could suppose that the aberration content does not vary with position. This compromise will allow one to recover a good quality image only in selected regions of interest, and we have to make sure that the size of these regions is at least equal to the characteristic size of the objects we wish to image. In order to obtain an estimate of the size of this surface, we measured the size of the isoplanatic

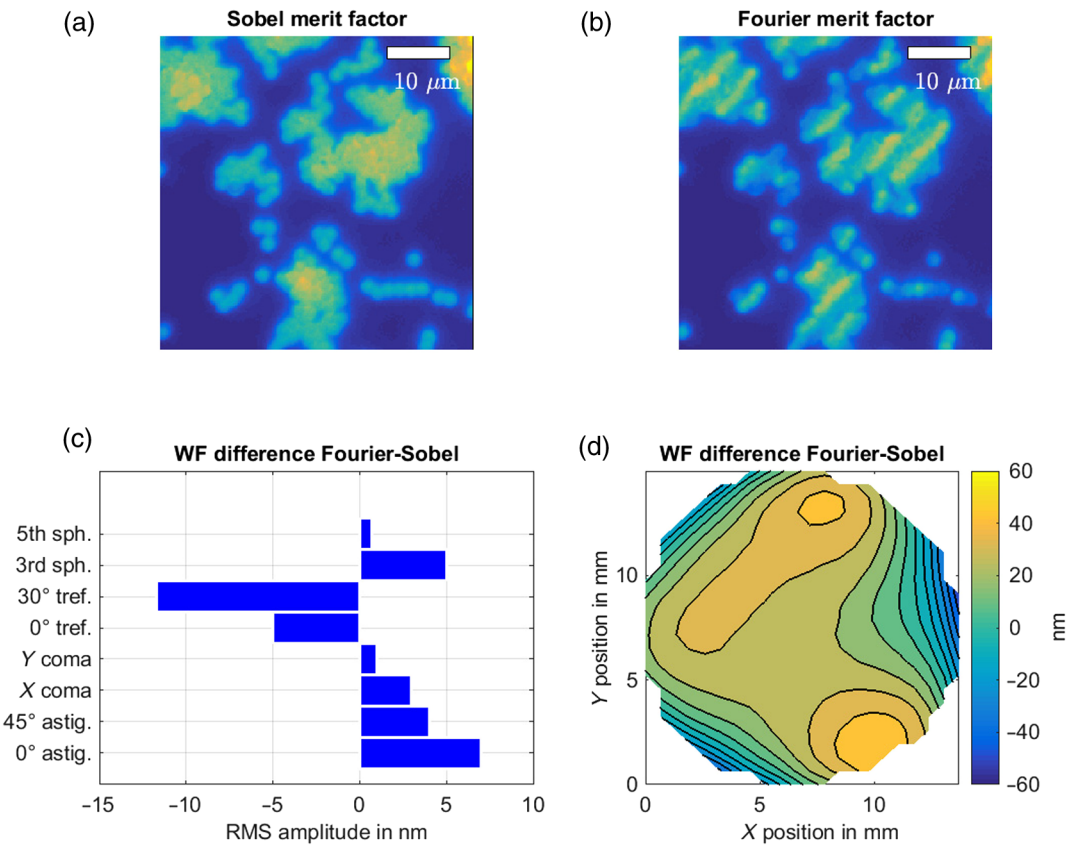

Fig. 2 Two different kinds of optimizations on images of a dense stripe of 1 μm green fluorescent beads embedded in an agarose gel. (a) Image with optimization based on Sobel merit factor. Scale bar: 10 μm. (b) Image with aberration correction based on Fourier merit factor. Scale bar: 10 μm. (c) Decomposition of the differential wavefront in terms of aberrations. (d) Differential wavefront for the DM shapes after Sobel and Fourier optimizations.

patch we could obtain with our setup with Strehl ratios' measurements.[20] We deposited 200-nm-diameter fluorescent beads on a coverslip and used the sensorless correction method on a single isolated bead with a Sobel merit factor. We determined the mirror shape that optimized the image of the beads at two different locations in the field of view: at the center and at upper left-hand corner of the camera field of view. We estimated the Strehl ratio of each bead of the field of view. The Strehl ratio is defined as the ratio of the peak intensity of the actual microscope point spread function over the peak intensity of the ideal microscope Airy spot. We evaluated the Strehl ratio of individual beads: we measured, for each bead image, the fraction of the total signal present in the brightest pixel. The results were then corrected to take into account the beads diameter, pixel size, magnification factor, and the distance between the beads images barycenter and the corresponding brightest pixel center. The Strehl map for the two mirror shapes is given in Figs. 3(a) and 3(b). Figure 3(c) shows beads close to the center of the corrected area and Fig. 3(d) shows beads 150 μm away from the center of the corrected area. In both cases, we obtained Strehl ratios larger than 0.6 on 100-μm-diameter discs around the fluorescent bead used as a guide star [Fig. 3(e)]. The isoplanatic area obtained with our modified microscope was smaller than the one of the original microscope, which covers most of the field of view. The added optical and mechanical elements were stock components. The full setup including the microscope could not be optically optimized and thus field-dependent aberrations were present. Despite this limitation, the size of this isoplanatic surface was compatible with the characteristic size of the structures we wanted to observe in our samples. We conclude that if we image regions of a size comparable to the isoplanatic surface, and if the aberration content is reasonably constant within this region, then the optimization loop based on a merit function will restore the quality of the image in the region of interest. In order to ensure that the wavefront correction did not induce any focus shift, we compared the position of the focal plane of our microscope with both best flat and optimized mirror shapes. We imaged a sample made of a single layer of 200 nm beads and computed the Sobel merit factor for different axial positions of this sample. The position at which the merit factor is lowest is considered as the best focus. We found a distance between the two best foci of 120 ± 60 nm, which is smaller than the depth of field of our objective.

3.3 *Evaluation of Axial Extension of Correction into Drosophila Brain*

The samples we wish to study being 3-D, we have to characterize the extension of the efficiency of the aberration correction in the axial direction, i.e., the one of the optical axis in our biological sample. We imaged *Drosophila melanogaster* brain *in vivo* and especially, a region called the mushroom bodies known to be the memory center of the fly[21] (see

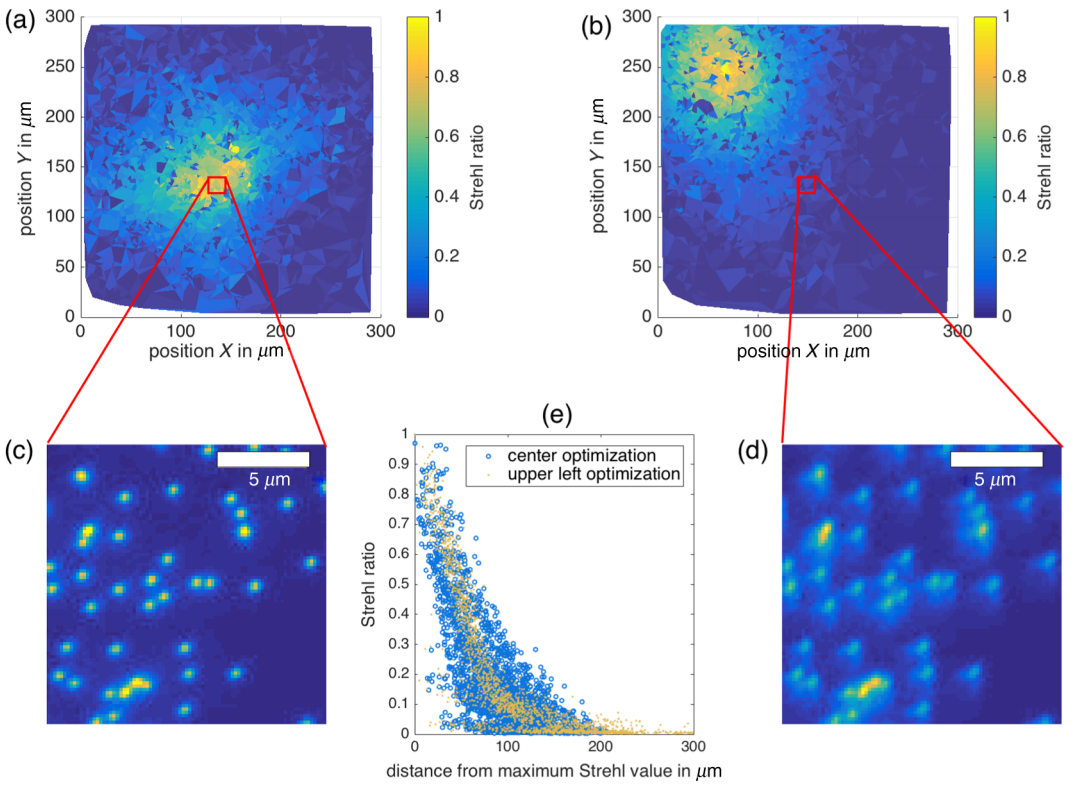

Fig. 3 Strehl ratios measurements. (a) Strehl map for an aberration correction on a bead in the center of the field of view. $n = 2382$ beads are used for the map reconstruction. (b) Strehl map for an aberration correction on a bead in the top left-hand corner of the field of view. $n = 2170$ beads are used for the map reconstruction. (c) Image of beads in the center of the field of view when the aberration correction is applied on a bead in the center of the field of view. Scale bar: 5 μm. (d) Image of beads in the center of the field of view when the aberration correction is applied on a bead in the top left-hand corner of the field of view. Scale bar: 5 μm. (e) Representation of the Strehl ratio with respect to distance to the maximum Strehl ratio value for the two different locations of correction in the field of view.

Sec. 2.1 for details about *in vivo* fly preparation for imaging). We projected a grid pattern of 2.5 μm period into the brain at different depths: 30, 40, and 50 μm below the brain surface. For each of the depths, we corrected optical aberrations and improved the grid contrast by running the optimization algorithm with Fourier merit factor. We then calculated the RMS amplitude of the grid pattern in the images by calculating the standard deviation of the difference of the two normalized images (with uniform and structured illumination). The results are presented in Fig. 4, where the depth of the focal plane is shown on the ordinate, and the depth at which the optimization was performed is on the abscissa. The best flat mirror shape corresponds to optimization at a depth of zero, where optimization was performed using the WS and fluorescent beads. The RMS amplitude is given as grey levels in the image. For example, the point where the contrast level is 132 corresponds to the case where the optimization step was performed 40 μm below the surface, but the image was recorded at 50-μm depth. With the best flat mirror, the grid RMS amplitude decreases very rapidly with depth inside the *Drosophila* brain. Below 30 μm into the brain, it becomes impossible to process structured illumination microscopy without adaptive optics. With aberration correction, we were able to improve the grid contrast down to 50 μm depth. For example, at 50 μm deep inside the *Drosophila* brain, we obtained a fourfold improvement of the grid RMS amplitude when the loop was run at the same depth compared to the case where we kept the best flat mirror. The contrast obtained, when the optimization was performed at the imaging depth, remains constant with increasing depth. This proves that the optimization should be able to preserve the image quality within thick samples. Comparison with the results obtained with the mirror shape optimized on the surface proves that without a depth dependant optimization, it is impossible to image structures deeper than a few tens of micrometers. Eventually, we observed that the grid contrast decreases by 20% if the optimization depth is 10 μm above or below the imaging plane. We took this value of 10 μm as a rough estimate of the thickness in which we could keep the same correction when performing 3-D imaging.

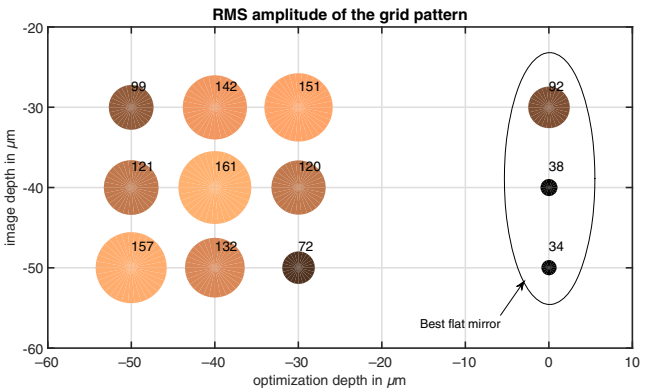

Fig. 4 Evaluation of the RMS amplitude of the grid pattern down to 50 μm inside the brain with the best flat mirror shape and with optimized DM shapes. Three different depths were imaged inside the *Drosophila* brain: 30, 40, and 50 μm under the brain surface. For each of these depths, we run the optimization algorithm with the Fourier merit factor to correct aberrations. To quantify the improvement brought by the adaptive optics on the quality of the patterned illumination, we calculated the RMS amplitude of the projected grid.

3.4 *Temporal Stability of Aberration Correction for In Vivo Imaging*

Our aim being to image living samples, the temporal behavior of the wavefront correction is a key issue. Indeed, if the aberrations are fluctuating, it will be necessary to run the optimization step at regular intervals. We evaluated the fluctuations of the optimized DM shape by imaging a fixed plane within the brain and running the optimization loop every 10 min for 1 h. We chose this duration because it corresponds to the typical duration of functional imaging experiments. The result is shown in Fig. 5 in which the change of the DM shape is presented as RMS values of the corrected aberrations. These corrections did not fluctuate by more than a few hundreds of nanometers. The third- and fifth-order spherical aberrations were particularly stable. We explain the erratic behavior of the 45-deg astigmatism, which fluctuates much more than all other aberrations, by observing that our Fourier merit factor optimizes only one particular region of the Fourier space. The effect of astigmatism on a microscope optical transfer function depends on orientation and has a moderate effect in a direction in the Fourier space.[22] If the region in the Fourier space, chosen for optimization and determined by the grid frequency and orientation, lies in the region where astigmatism, either at 0 or 45 deg, has little effect, then the merit factor is poorly sensitive to its presence. Therefore, variation of astigmatism cannot be attributed to the sample evolution. These measurements suggest that aberrations induced by the *Drosophila* brain are static.

3.5 *Dependence on the Spatial Frequency of the Illumination Pattern*

We tested the influence of the choice of the pattern frequency on the Fourier merit factor. We compared the results of optimizations performed at the same location in a sample but with two different pattern periods of 1.25 and 2.5 μm. These two frequencies of the pattern were chosen because they were well suited to Kenyon cells imaging into *Drosophila* brain. Figure 6 shows the difference between the two DM shapes expressed as RMS difference of the optimized aberrations. Except for the 45-deg astigmatism, all the aberrations were corrected to <100 nm. Here also, the pattern orientation makes the Fourier merit factor less sensitive to 45-deg astigmatism than to 0-deg astigmatism.

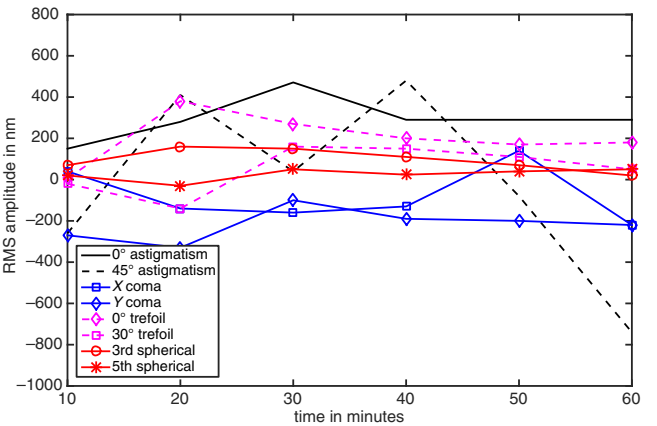

Fig. 5 Temporal evolution of RMS amplitude of third-order aberrations and fifth-order spherical aberration for a 30-μm imaging depth inside living *Drosophila* brain.

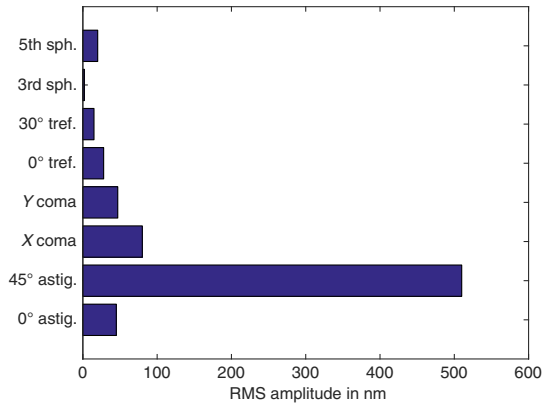

Fig. 6 Differential aberration content for optimizations with two different grid periods: 1.25 and 2.5 μm in the sample, for a 40-μm imaging depth inside living *Drosophila* brain.

The correction does not depend on the choice of one or the other of the two tested frequencies.

4 Biological Results: HiLo Imaging in Depth Inside In Vivo *Drosophila* Brain

The quality of the optical sections in structured illumination microscopy, particularly their low spatial frequency content, depends mainly on the contrast of the illumination pattern. Indeed, this contrast is the weight of the frequency shifted spectra of the samples that are used in the HiLo algorithm. If the grid contrast is too low, then the low spatial frequency content that the sectioning algorithm aims at recovering will be polluted by some high-frequency content of the unmodulated spectrum. Before computing optical sections, we present the effect of our optimization method on the illumination pattern. We have reproduced the following experiments on four flies and we present the results obtained with one of them. We performed optimization based on Fourier merit factor at 40 μm deep inside the *Drosophila* brain tagged with GFP biosensor. Without adaptive optics, the grid quality was very poor [Fig. 7(a)] and could be improved by running the optimization algorithm taking into account all the third-order aberrations and the fifth-order spherical aberration [Fig. 7(b)]. To emphasize the enhancement of the grid contrast with the aberration correction and make it more visible in the presented images, we decided not to present the raw images taken with structured illumination but we subtracted the uniform illumination image from the one with structured illumination. In order to cancel the proper axial displacements of the *Drosophila* brain during the course of the experiment, we compared the result of the optimized structured illumination image with an 80-μm-thick stack of images acquired every micrometer and obtained without optimization. We found the best corresponding image in this stack. The results presented show the same axial position in the brain. The radial power spectra, shown in Fig. 7(c), were determined by calculating the power in concentrical rings into the Fourier diagram of both images acquired with the best flat mirror and the optimized

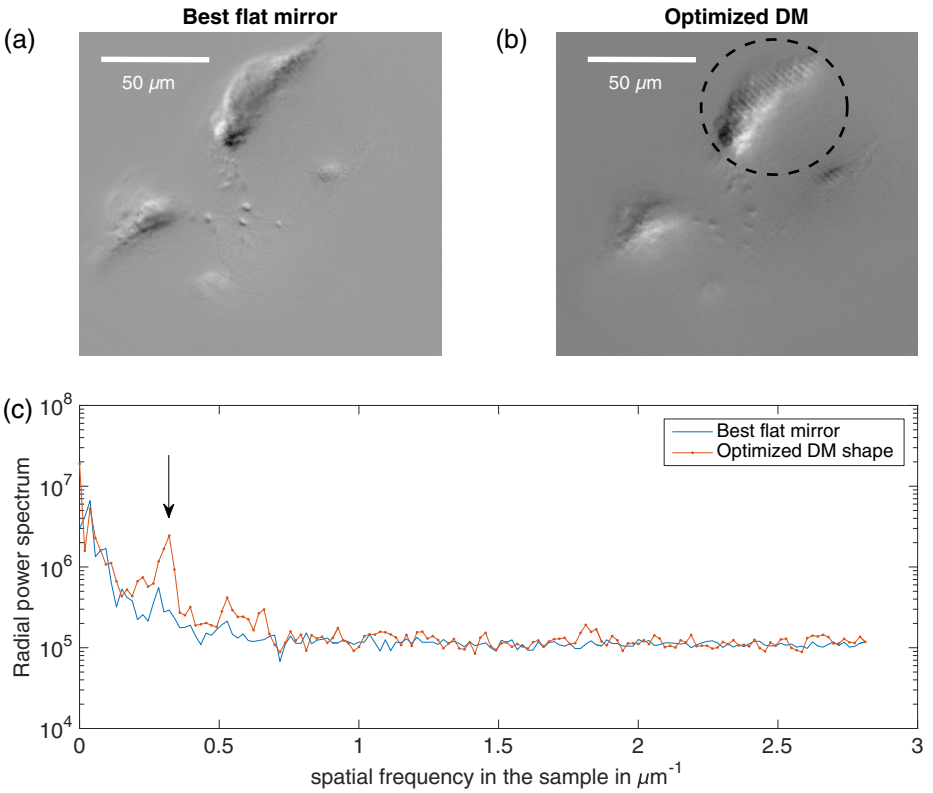

Fig. 7 (a) Processed fluorescence structured illumination image of mushroom bodies neurons obtained with the best flat mirror shape. (b) Processed fluorescence structured illumination image of mushroom bodies neurons obtained with the optimized mirror shape. Image processing consists in uniform illumination image subtraction. The encircled area corresponds to the region of interest, which has been optimized. The size of the images shown in (a) and (b) is 164×164 μm. (c) Radial power spectra of images shown in (a) and (b). The arrow points on the grid pattern spatial frequency.

mirror shapes. The peak, corresponding to the spatial frequency of our grid pattern, was only well resolvable when aberrations are corrected. This result proves once again that structured illumination microscopy cannot be performed at 40 μm inside *Drosophila* brain without the implementation of a corrective setup. It appears that this merit factor mimics a single guide star in Fourier space. Indeed, it points at a single spatial frequency $(f_{x,\mathrm{mod}}, f_{y,\mathrm{mod}})$ and aims at optimizing the frequency content of the images around this frequency. It is the Fourier equivalent of having a single guide star a location $(x_{\mathrm{star}}, y_{\mathrm{star}})$ in real space and optimizing the wavefront around this location. Thus, it suffers the same limitation of having a limited corrected frequency range equivalent of the isoplanatic surface in real space. This effect is apparent in Fig. 7(c), where the optimization process enhances the presence of the modulation pattern and drags the surrounding part of the spectrum. Frequencies far from the modulation frequency were less affected by the optimization.

We processed HiLo reconstruction at 40μm inside *Drosophila* brain. The results are shown in Figs. 8(a) and 8(b). The optical sections were built by combining the high spatial frequency content of a high-pass filtered flat illumination image and the in-focus low-frequency content.[2,4] The in-focus low-frequency content was obtained by demodulating and low-pass filtering the patterned image. The two image sets used to build the HiLo sections were taken 18 s apart. In order to verify that the differences between the two Hilo sections were not due to structural modifications of the brain, we acquired a third set of images with the correction removed and obtained a HiLo section identical to the initial one. To quantify the improvement of the quality of optical sections with adaptive optics, we plotted intensity profiles through HiLo images both for best flat mirror shape and optimized mirror shape [see Fig. 8(c)]. Due to a better grid contrast into the sample, we were able to recover in-focus low spatial frequencies. We calculated the radial power spectra for HiLo reconstruction with the best flat mirror, HiLo reconstruction with optimized mirror, flat illumination image with optimized mirror, and high spatial frequency content of flat illumination image with optimized mirror shape. All these four spectra superimpose for high spatial frequencies information [see Fig. 8(d)], but the low spatial frequencies content of images varies. The comparison of

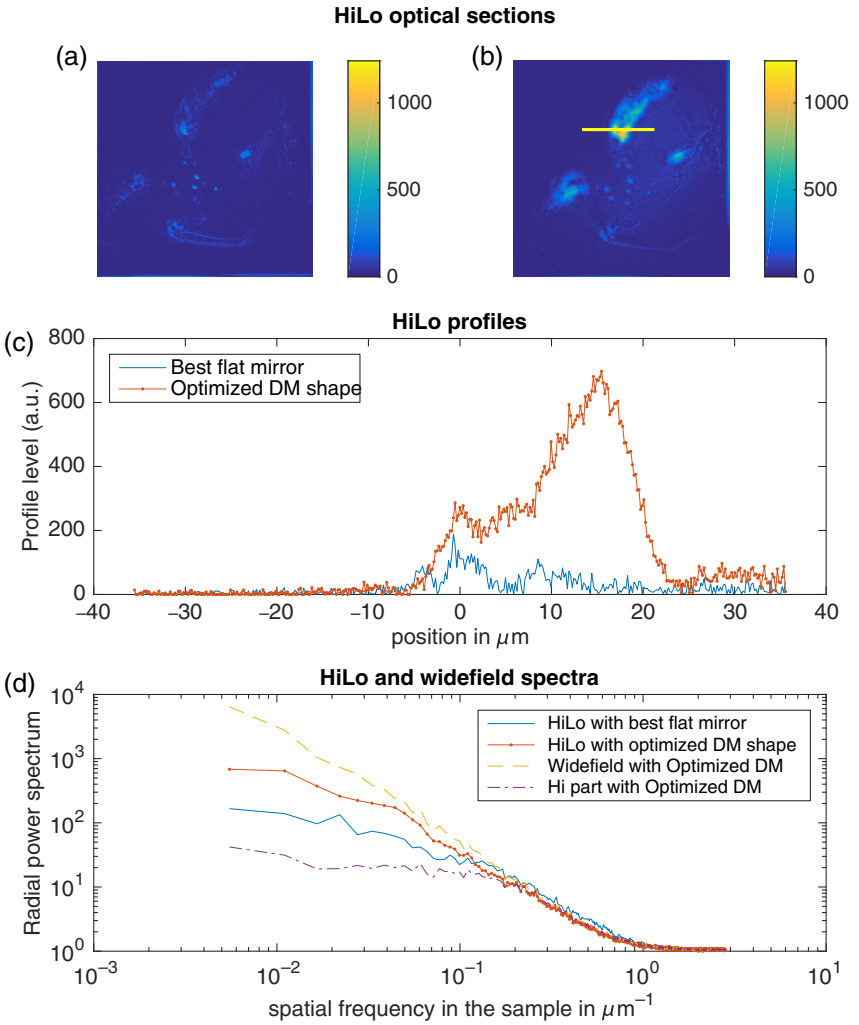

Fig. 8 HiLo imaging at 40 μm inside *Drosophila* brain. (a) HiLo reconstruction with the best flat mirror shape. Image size is 164×164 μm. (b) HiLo reconstruction with optimized DM shape. (c) Intensity profiles of HiLo images with best flat and optimized mirror shapes. (d) Radial power spectra in spatial frequency domain for HiLo image with the best flat mirror shape, HiLo image, widefield image and Hi part with optimized DM shape. Hi part denotes high-frequency content of widefield image.

the uniform illumination image spectrum and the HiLo image spectrum recorded with an optimized mirror shape clearly shows the removal of low-frequency content, this part being out-of-focus. Comparison of the two HiLo image spectra recorded with optimized and flat mirror shape proves that if the optimized mirror is not used then the HiLo algorithm cannot recover the in-focus low-frequency content. These results demonstrate that the capability of HiLo microscopy to recover in-focus low-frequency content in optical sections can be obtained at least 40-μm deep in living tissues but requires the use of a wavefront correction system acting on both the illumination and emission paths.

5 Conclusion

The results presented in this paper pave the way toward dynamical studies several tens of micrometers deep inside living samples. Nevertheless, degradation due to photobleaching can become a limiting factor. Due to the widefield optical sectioning technique that requires a low excitation illumination power, photobleaching was not observed during an optimization calculation loop (typically 0.5 s for one aberration mode with 100-ms exposure time on camera) and does not lead to variation of the merit factor, which used to determine the best DM shape. This optimization time and the correction quality depend on the number of aberrations, which are corrected. The best compromise that we experimentally determined consists in correcting all the third-order aberrations and the fifth-order spherical aberration. No significant grid contrast gain could be observed with higher orders aberrations correction while increasing optimization calculation duration and photobleaching.

We have proved that HiLo optical sections can be obtained deep inside living *Drosophila* brains and that the aberrations induced by the brain are static. We can thus think of ways to build stacks of optical sections throughout the whole brain. One way to build such a 3-D stack at a fast pace would be to record the optimized mirror shape every 10 μm into the brain in a first step and then to feed the DM with these shapes to perform fast HiLo microscopy at different depths. The optimization and imaging steps being decoupled, two different markers could be used and so the long optimization step would not lead to photobleaching of the markers used for HiLo microscopy.

Acknowledgments

This work was supported by a grant from Région Ile-de-France (project "ImPhysBio"). We would like to thank also T. Préat's laboratory for providing us with biological samples and X. Levecq and G. Clouvel from Imagine Optic Company for technical help and fruitful discussions.

References

1. L. Kong et al., "Continuous volumetric imaging via an optical phase-locked ultrasound lens," *Nat. Methods* **12**(8), 759–762 (2015).
2. J. Mertz and J. Kim, "Scanning light-sheet microscopy in the whole mouse brain with HiLo background rejection," *J. Biomed. Opt.* **15**(1), 016027 (2010).
3. S. Santos et al., "Optically sectioned fluorescence endomicroscopy with hybrid-illumination imaging through a flexible fiber bundle," *J. Biomed. Opt.* **14**(3), 030502 (2009).
4. A. Masson et al., "Micromirror structured illumination microscope for high-speed in vivo drosophila brain imaging," *Opt. Express* **22**(2), 1243–1256 (2014).
5. M. J. Booth, "Adaptive optics in microscopy," *Philos. Trans. R. Soc. A* **365**(1861), 2829–2843 (2007).
6. M. J. Booth, "Adaptive optical microscopy: the ongoing quest for a perfect image," *Light Sci. Appl.* **3**, e165 (2014).
7. J. M. Girkin, S. Poland, and A. J. Wright, "Adaptive optics for deeper imaging of biological samples," *Curr. Opin. Biotechnol.* **20**, 106–110 (2009).
8. P. Vermeulen et al., "Adaptive optics for fluorescence wide-field microscopy using spectrally independent guide star and markers," *J. Biomed. Opt.* **16**(7), 076019 (2011).
9. O. Azucena et al., "Wavefront aberration measurements and corrections through thick tissue using fluorescent microsphere reference beacons," *Opt. Express* **18**(16), 17521–17532 (2010).
10. O. Azucena et al., "Adaptive optics wide-field microscopy using direct wavefront sensing," *Opt. Lett.* **36**(6), 825–827 (2011).
11. D. Débarre et al., "Adaptive optics for structured illumination microscopy," *Opt. Express* **16**(13), 9290–9305 (2008).
12. J. B. Duffy, "Gal4 system in drosophila: a fly geneticist's Swiss army knife," *Genesis* **34**(1–2), 516–529 (2002).
13. R. I. Wilson, G. C. Turner, and G. Laurent, "Transformation of olfactory representations in the drosophila antennal lobe," *Science* **303**(5656), 366–370 (2004).
14. D. Débarre, M. J. Booth, and T. Wilson, "Image based adaptive optics through optimisation of low spatial frequencies," *Opt. Express* **15**(13), 8176–8190 (2007).
15. J. A. Kubby, *Adaptive Optics for Biological Imaging*, CRC Press, Boca Raton (2013).
16. D. Karadaglica and T. Wilson, "Image formation in structured illumination wide-field fluorescence microscopy," *Micron* **39**(7), 808–818 (2008).
17. J. C. Dainty, *Adaptive Optics in Optical Imaging and Microscopy*, P. Torok and F. J. Kao, Eds. Springer, Berlin (2003).
18. D. Burke et al., "Adaptive optics correction of specimen-induced aberrations in single-molecule switching microscopy," *Optica* **2**(2), 177–185 (2015).
19. J. Mertz, H. Paudel, and T. G. Bifano, "Field of view advantage of conjugate adaptive optics in microscopy applications," *Appl. Opt.* **54**(11), 3498–3506 (2015).
20. M. Born and E. Wolf, *Principles of Optics*, 7th ed., Cambridge University Press, Cambridge, UK (1999).
21. M. Heisenberg, "Mushroom body memoir: from maps to models," *Nat. Rev. Neurosci.* **4**(4), 266–275 (2003).
22. B. Y. Gerlovin and N. A. Istomina, "Method of calculating the optical transfer function for astigmatism and defocusing," *J. Opt. Technol.* **69**(9), 640–643 (2002).

Mélanie Pedrazzani obtained a PhD in physics in 2015 from the Université Paris Saclay (Orsay). She received her MSc in optics from the Université Paris Sud in 2012. Her research focuses on neuroscience with imaging of *Drosophila* brain *in vivo* and adaptive optics for structured illumination microscopy.

Vincent Loriette is a research scientist at the Laboratoire de Physique et d'Etude des Matériaux at ESPCI (Paris). He received his PhD in astrophysics in 1995 from Université Denis Diderot under the supervision of Claude Boccara. Until 2007, he was developing the optical metrology instruments for the Virgo project (gravitational wave detector). He is currently developing fluorescence microscopes with extended spatial resolution or wide-field optical sectioning properties.

Alexandra Fragola is an assistant professor at Pierre et Marie Curie University, where she obtained a PhD in 2003 under the supervision of Claude Boccara and Lionel Aigouy in near-field microscopy. At the Laboratoire de Physique et d'Etude des Matériaux, she is currently developing super-resolution fluorescence microscopes for live cell and *in vivo* imaging, using time-gated detection, structured illumination techniques, and adaptive optics.

Biographies for the other authors are not available.